

# Diffusion as a Ruler: Modeling Kinesin Diffusion as a Length Sensor for Intraflagellar Transport

Nathan L. Hendel,<sup>1,2</sup> Matthew Thomson,<sup>3</sup> and Wallace F. Marshall<sup>1,\*</sup>

<sup>1</sup>Department of Biochemistry and Biophysics and <sup>2</sup>Bioinformatics Graduate Group, University of California, San Francisco, San Francisco, California; and <sup>3</sup>Division of Biology and Biological Engineering, California Institute of Technology, Pasadena, California

**ABSTRACT** An important question in cell biology is whether cells are able to measure size, either whole cell size or organelle size. Perhaps cells have an internal chemical representation of size that can be used to precisely regulate growth, or perhaps size is just an accident that emerges due to constraint of nutrients. The eukaryotic flagellum is an ideal model for studying size sensing and control because its linear geometry makes it essentially one-dimensional, greatly simplifying mathematical modeling. The assembly of flagella is regulated by intraflagellar transport (IFT), in which kinesin motors carry cargo adaptors for flagellar proteins along the flagellum and then deposit them at the tip, lengthening the flagellum. The rate at which IFT motors are recruited to begin transport into the flagellum is anticorrelated with the flagellar length, implying some kind of communication between the base and the tip and possibly indicating that cells contain some mechanism for measuring flagellar length. Although it is possible to imagine many complex scenarios in which additional signaling molecules sense length and carry feedback signals to the cell body to control IFT, might the already-known components of the IFT system be sufficient to allow length dependence of IFT? Here we investigate a model in which the anterograde kinesin motors unbind after cargo delivery, diffuse back to the base, and are subsequently reused to power entry of new IFT trains into the flagellum. By mathematically modeling and simulating such a system, we are able to show that the diffusion time of the motors can in principle be sufficient to serve as a proxy for length measurement. We found that the diffusion model can not only achieve a stable steady-state length without the addition of any other signaling molecules or pathways, but also is able to produce the anticorrelation between length and IFT recruitment rate that has been observed in quantitative imaging studies.

two possibilities

## INTRODUCTION

How does the cell control the size of its organelles? This question has been puzzling cell biologists for decades. Cells must have a robust and efficient procedure for building organelles with a specific size and shape. The stochastic kinetics of polymerization typically leads to formation of structures with widely varying sizes in the absence of any size-dependent assembly or disassembly processes (1). But organelles are thousands of times bigger than the materials used to build them, so how can molecular pathways of assembly sense and respond to organelle size to yield organelles of a necessary size for proper function? This problem is extremely difficult to solve in the general case considering the many different types of organelles and their often highly complex structures. To simplify the problem, we will just consider the eukaryotic flagellum. Flagella (also known as “cilia”) are long whiplike appendages protruding from

certain cells and are used for both locomotion and sensing. Unlike a prokaryotic flagellum, which is made of a tube of a single polymer, the eukaryotic flagellum is a more complex structure made of nine microtubule doublets underlying a protrusion of the plasma membrane. These doublets are nucleated by the basal body. The flagellum is the perfect organelle to model mathematically because it has a linear geometry: when it grows, it gets longer but not wider, making it essentially a 1D organelle.

structure of the model



Here, we will consider the flagella of *Chlamydomonas reinhardtii*, a eukaryotic alga that has two flagella. When *Chlamydomonas* develop, their flagella grow with decelerating kinetics, ultimately leveling out to a steady-state length (2). This slow-down in growth suggests that some part of the flagellum-building mechanism is feedback-regulated by length such that growth ceases when the flagellum reaches a certain length. In cells with two flagella, an interaction is observed such that when one flagellum is severed, the other flagellum will shorten until the two flagella reach the same length (2). This length equalization also suggests some form of feedback control between the two flagella.

reason for choosing this model



Submitted June 29, 2017, and accepted for publication November 29, 2017.

\*Correspondence: [wallace.marshall@ucsf.edu](mailto:wallace.marshall@ucsf.edu)

Editor: David Odde.

<https://doi.org/10.1016/j.bpj.2017.11.3784>

© 2017 Biophysical Society.

This is an open access article under the CC BY-NC-ND license (<http://creativecommons.org/licenses/by-nc-nd/4.0/>).



## objective of the study

This study examines how these types of length-dependent control of assembly might happen.

Most of the flagellum-building machinery is known. To build a flagellum, cells use a process called “intraflagellar transport” (IFT) (3–6). IFT, diagrammed in Fig. 1 A, is mediated by complexes of ~20 polypeptides called “IFT proteins”, which contain numerous protein-protein interaction domains capable of binding the building blocks of flagella such as tubulin and axonemal dynein arms. These IFT protein complexes associate into linear arrays known as “trains” (7,8). IFT trains are pulled to the distal tip by heterotrimeric kinesin-2 motors (9,10). Upon reaching the tip, the contents of the cargo add to the length of the flagellum. Flagella are thus undergoing continuous incorporation of new tubulin and other building blocks. To counter this, tubulin is continually removed from the flagellar tip at a constant, length-independent rate (11). Because this decay rate is constant, to achieve a steady state, the rate of IFT must be length-dependent (11,12).

IFT trains are recruited from docking sites on the basal bodies (13) into the flagellum to begin transport through a process called injection. The physical mechanism of injection is unknown, but it is thought to involve IFT trains moving through some sort of selective pore or barrier similar to a nuclear pore (14,15). Although the molecular details of the injection process remain unclear, quantitative imaging studies (16) have revealed that motors are recruited into the flagellum according to a pattern of dynamics similar to how sand dropped onto a sandpile will fall off (avalanche) if the pile is high enough. For example, the more time elapses before a train is injected, the larger the train is, and the

## biological model for the start of the trains

get more info on power-law and avalanching systems

larger a train is injected, the more time will elapse before the next injection event. The sizes of the injection events are power-law distributed, similar to the size of avalanching events in sandpiles and other avalanching systems. These similarities suggest a simple model in which IFT proteins and motors accumulate at the basal body, gradually exerting more force on the pore until eventually a cluster of motors pushes through the pore, injecting a train (16). In such a scenario the rate at which motors accumulate at the base would ultimately be what determines the rate of injection.

Quantitative live cell imaging (16,17) has shown that the rate of injection of motors is anticorrelated with the length of the flagellum. Furthermore, quantitative analysis of IFT cargo loading suggests that cargo loading is also length-dependent (18). These length-dependencies imply some kind of communication between the base and the tip. Perhaps some sort of additional signaling pathways have evolved that can sense length, transduce length into some form of molecular signal, and then use this signal to modulate the injection of IFT proteins at the base of the flagellum. Several possible models for length-sensing pathways have been described and analyzed (16,19). Each of these models invokes additional molecular pathways that could transduce length into a signal that would gate entry of IFT particles through a pore. But what if no such additional pathway exists? Might the IFT machinery itself be capable of responding to changes in flagellar length?

Here we consider a model that takes into account the return of IFT motors from the flagella tip. IFT is a cyclical process: IFT trains and motors move to the tip, deliver cargo, return to the cell body, and then are reinjected (20). Experimental

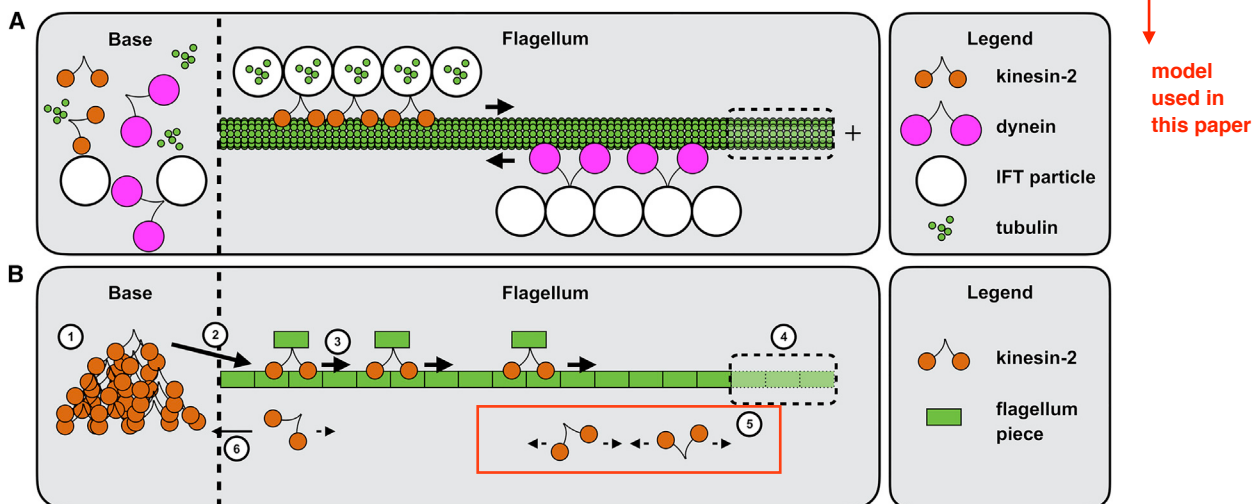


**FIGURE 1** Agent-based model of IFT. (A) Diagram of IFT. Kinesin-2 motors form trains that carry IFT particles containing tubulin to the plus-end of the microtubule bundle, the tip of the flagellum. Dynein motors carry the IFT particles back to the base. (B) Model version of IFT. Kinesin motors pile up at the base (1), and once the pile is large enough, some are injected into the flagellum with cargo (2). Each motor constantly moves toward the tip of the flagellum (3). Once they reach the end, they flagellum gets longer (4), and the kinesin motors unbind and diffuse (5). Once they diffuse back to the base, they are absorbed and reenter the pile in the base (6). While this is happening, the flagellum is shrinking at a length-independent rate. To see this figure in color, go online.

questions specific  
to this article

studies have addressed how motors are recruited into the flagellum, how motors get to the tip, and how the flagellum grows and shrinks. Two aspects of the IFT system that have been less intensively studied are how motors are sent to the pool at the basal body and what happens to the anterograde kinesin motors after they deliver their cargo to the tip.

We propose a simple model to answer both of these questions: after dropping off their cargo, the kinesin motors unbind and diffuse back to the base, where they are then added back into the pool of accumulated motors waiting to be injected. The initial evidence for a diffusive return of the kinesin motor was the failure to observe processive retrograde traces in kymographs of IFT using GFP-tagged kinesin subunits (17), and the fact that

- #1 when retrograde IFT is inhibited, IFT proteins accumulate at the flagellar tip, but the kinesin motor does not (21). Direct tracking of individual trains by a novel bleach-gate method
- #2 has shown that kinesin undergoes diffusion after dissociation from trains at the distal tip (22). In considering simple models for IFT that incorporate diffusive return of kinesin, we observed that the rate of diffusive return of kinesin motors

to the pool at the flagellar base can serve as a proxy for flagellar length measurement, leading us to propose that the diffusion of the IFT kinesin motor may, itself, be the long-sought length sensor that regulates IFT injection. The complicating factor in such a model is that the source of the diffusing molecule, kinesin, is itself dependent on the rate of injection,

which in turn is dependent on the rate of diffusive return. This mutual feedback between injection and return raises the question of whether such a system is capable of stably achieving a unique length at steady state. It is also not obvious how this type of system will perform when two flagella are considered simultaneously.

In this article, we investigate this hypothesis using a fine-grained agent-based model that is analyzed using computer simulations together with a coarse-grained differential equation model that can be solved analytically. In the agent-based model, we explicitly model the flagellum and motors and run time-dynamics simulations. In the differential equations model, we solve the steady-state form of the diffusion equation with boundary conditions that incorporate active delivery of IFT to the tip and a diffusive return to the base. Each model is detailed below. The result of our analysis is that diffusive return of kinesin, when combined with a simple model for IFT-mediated flagellar assembly, does indeed predict a stable flagellar length control system capable of achieving a unique steady-state length and of equalizing the lengths of flagella in a biflagellate cell, without the need to add any additional components beyond what is already known from prior studies of IFT.

## MATERIALS AND METHODS

Agent-based models described in Results were implemented using Python's built-in object oriented methods. Plots were generated within a Jupyter Notebook framework.

## RESULTS

### Agent-based model

Tools: python simultaia

As a starting point to look for potential length dependencies in the IFT system, we implemented a simplified model of the individual components of the system (Fig. 1 B) and asked what predictions this model might make about length dependence. We built an agent-based model to simulate kinesin and microtubule growth dynamics through stochastic rules grounded in biochemistry. Specifically, we used the software Python's built-in object-oriented programming methods (<https://www.python.org/doc/>) to explicitly model individual motors and the flagellum they populate.

The flagellum has attributes such as length and environmental variables that include the decay rate and diffusion coefficient. Each motor has attributes including position, transport speed, a Boolean to indicate whether it is in the flagellum or in the base, and another Boolean to indicate whether it is bound (in active transport) or unbound (diffusing) if it is in the flagellum. To simulate dynamics,

we cycle through each motor and test a series of conditionals to determine how it should adjust its position. If it is on the flagellum and bound, its position increases by a constant. If its position reaches the flagellum's length, indicating that it has reached the tip of the flagellum, it unbinds (changes its state from active transport to diffusion), and the flagellum grows by the designated growth increment. If it is in the flagellum and unbound, it moves randomly to the left or to the right. If it is unbound and reaches the base, it is absorbed into the base and becomes inactive. At each time step, we count the number of motors in the base, and if that value is greater than a variable for avalanche threshold, we use a Weibull distribution to determine how many avalanche-out and move into the flagellum, and reactivate into active transport. We chose a Weibull distribution because it can fit the long-tailed distribution of train sizes that have been experimentally determined (16). The Weibull distribution has a multiplicative constant that we set to the difference between the number of motors in the base and the threshold for avalanching, plus a constant we could vary. Meanwhile, at each time step, the flagellum shrinks by the decay rate constant. Table 1 lists the parameters we used, and how we obtained the values used for simulation.

TABLE 1 Parameters Used in Agent-Based Model

Parameter	Default Value	How Value Was Obtained
Number of motors	200	Marshall and Rosenbaum (11)
Active transport speed	2 $\mu\text{m/s}$	Chien et al. (22)
Growth size per motor	1.25 nm	Marshall and Rosenbaum (11)
Decay rate	0.01 $\mu\text{m/s}$	Marshall and Rosenbaum (11)
Diffusion coefficient	1.75 $\mu\text{m}^2/\text{s}$	Chien et al. (22)
Weibull distribution power	2.85	Ludington et al. (16)
Weibull distribution prefactor	10	Arbitrary
Avalanche threshold	30 motors	Ludington et al. (16)

model for flagellum

modle for motor

framework for the simulation

motors

```

1 is on flag + is bound:
-> pos += const
2 is at the tip of flag:
->unbinds
flag += const
3 is in flag + unbound:
-> moves rand R or L
4 if its unbound + base:
-> reabsorbs and inactive

```

check if  
motor at  
base ar  
sufficient to  
lunch an  
avalanche

get more info

assumption ->  
limitation?

It is important to note that this model does not specifically represent the IFT particles. It is assumed that each motor is associated with an IFT particle carrying a fixed quantity of material, as represented by the growth size per motor.

This model lets us consider the journey of a single motor (Fig. 2 A). In the example shown, it starts in active transport at position zero. The conditional that checks if it is bound commands its position to increase by the active transport step size. This process continues until the position of the motor is equal to the length of the flagellum. This position represents the tip, and at this stage, the motor's bound parameter is changed to False (representing diffusion), and the length of the flagellum is increased by the build size parameter. In the next time step, the conditional that checks if the motor is bound sees that it is not bound, and this time it adjusts its position by the root mean square diffusion length multiplied by either 1 or  $-1$ , determined randomly. This

simulates the randomness of diffusion. Once its position reaches zero (the base), its Boolean value stating whether it is in the flagellum is set to False to indicate absorption to the basal pool. Every time step, a random power-law number generator determines how many motors that are inactive at the base are injected onto the flagellum. If that number is zero, or if it is nonzero but this motor is not among those injected, this motor will stay stationary at position zero. Once it gets injected, it goes back into the flagellum in active transport, and the entire process repeats for the remainder of the simulation. By simulating many motors within the same flagellum (each adding length to the flagellum upon reaching the tip and then diffusing back), combined with constant shortening of the flagellum, we can simulate the overall growth dynamics of a single flagellum (Fig. 2 B). Simulations over time show that this system allows the flagellum to grow to a defined length with decelerating kinetics.

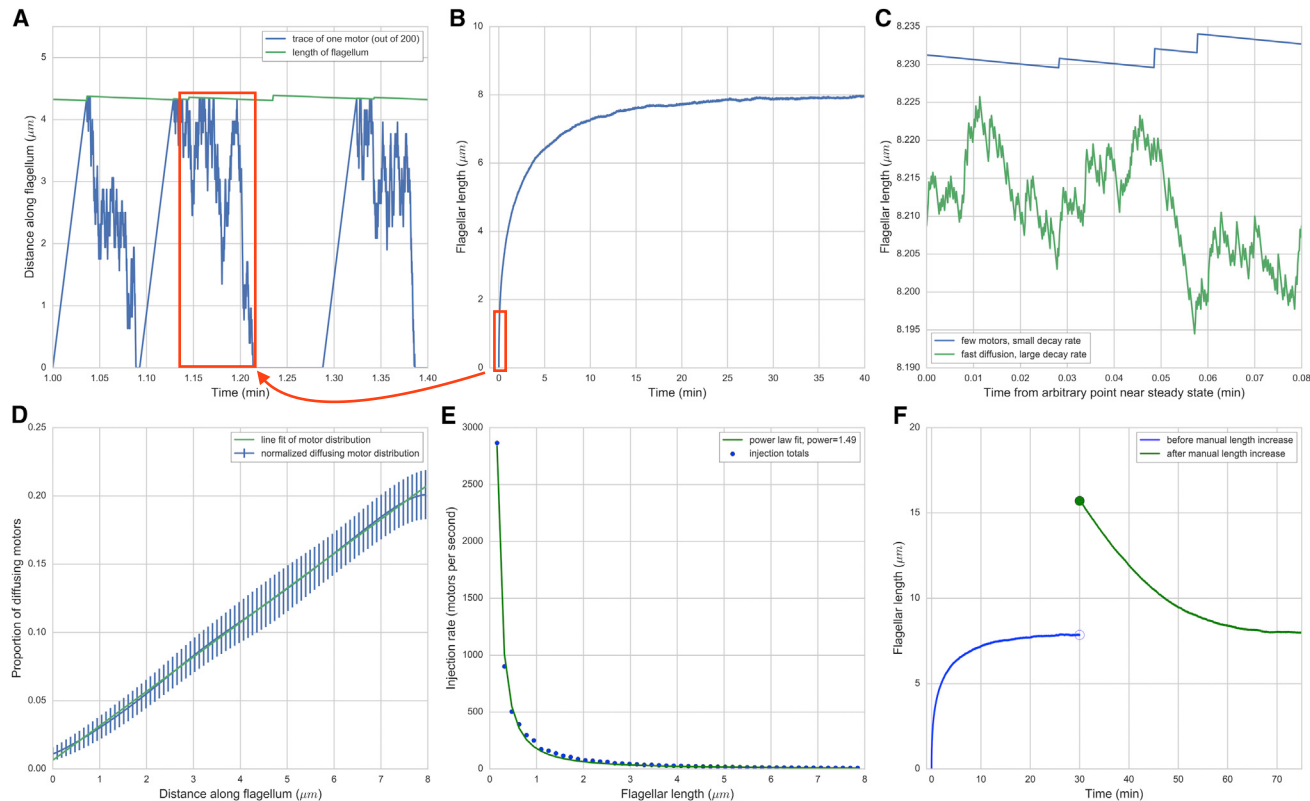


**FIGURE 2** Results of agent-based simulation. (A) Blue: Shown here is the journey of a single motor in a zoomed-in window of the flagellum's early growth. Green: Shown here is the flagellar length. (B) Given here is flagellar length over time in simulated minutes. (C) Shown here is the expanded window of two simulated flagella's lengths over time as they approach steady state. The blue trace is for a flagellum with a small number of motors and a small decay rate, and the green trace is for a flagellum with a larger number of motors, larger diffusion coefficient, and larger decay rate. The standard deviation of the blue trace is  $1.40 \text{ } \mu\text{m}$ ; the standard deviation of the green trace is  $6.69 \text{ } \mu\text{m}$  in the time frame shown. (D) Blue: Given here is the distribution of diffusing motors along flagellum using the average of 103 simulations with identical parameters and a Gaussian kernel density function applied to the means at each position. Green: Given here is the linear fit. (E) Plot of injection size is given as a function of flagellar length. The points were generated by simulating 10 cells, taking their injection times and sizes, and binning them into measurements of average injection size per unit time in each of the 50 evenly spaced bins. (F) Given here is a demonstration of the stability of the length control system. Plot shows simulation in which length was manually increased to double its steady-state length at  $t = 30$  min. Blue shows before the manual increase and green shows after, showing restoration to initial steady-state length. The time step in each simulation was 0.01 s. To see this figure in color, go online.

as expected flag length fluctuate around steady state  
-> fluctuations (but not the steady length) depends on parameters of the simulation



assumption: the stady state is achived much faster than change in length of the flagellum

Diffusion as a Ruler

Because motors undergo random motion as they return and are released from the base in a way that depends on the time history of their return, it is expected that flagellar growth rates will fluctuate, and indeed our simulations confirm that the length does indeed fluctuate around a steady-state average length. We found that the magnitude of this fluctuation varied between simulated flagella with different parameter values even if they reach the same steady-state length (Fig. 2 C), indicating that fluctuation contains additional information about the system beyond what the steady-state length provides. By counting motors in different states, we can ask how the pool of diffusing motors is distributed along the length. We find that the probability of finding a motor at a given distance from the tip is approximately linear, consistent with the expected form of a diffusional gradient with a source at one end and a sink at the other at steady state (Fig. 2 D).

Having found that the simple agent-based model of diffusive kinesin return is able to produce a defined flagellar length, the key question is whether the length-dependence of IFT injection can be recapitulated. As shown in Fig. 2 E, the average injection size per unit time of injected IFT trains in the simulation shows an inverse dependence on flagellar length, as previously reported in experimental measurements (16,17).

The length control system modeled here is stable, as indicated by simulated experiments in which the length is transiently perturbed. As illustrated in Fig. 2 F, a transient externally imposed elongation of a flagellum at steady state, achieved by simply resetting the length to a longer value, is followed by a shortening back to the steady-state length. This implies that the steady-state length is determined by the input parameters rather than the transient state of the flagellum.

## Dependence of length on model parameters

The agent-based model described above is a minimalist representation of the IFT system, but whereas our simulations show that stable length is achieved, it is not obvious from the successful simulations why the model works or how the parameters of the model contribute to the value of the steady-state length. To gain a physical understanding of how this model achieves length control, we investigated a more idealized model that will allow us to solve for the steady-state solution analytically. By reducing the model to a classical boundary value problem, we can solve for system behavior as a function of key parameters in closed form. If we make the assumption that active transport time and expected time delay of injection is small relative to the timescale of diffusive return, we can model this system as a diffusion problem with a constant source of free motor protein at the tip of the flagellum and a sink at the base. If we also assume that no diffusing motors rebind to the flagellum, we can apply Fick's first law of diffusive flux in steady state.

This law strictly applies to steady state, but we can still use it to study the dynamics of flagellar growth by invoking a separation of timescales. We assume that the timescale of flagellar length changes due to growth and shrinkage (which happens on the timescale of minutes to hours), is slow relative to the timescale over which diffusion establishes a stable gradient, such that the system can be viewed as being in a quasi-steady state. (This is similar to the classic statistical mechanics problem of slowly expanding a box containing gas: when the expansion of the box is slow, the system is reversible and equilibrium statistical mechanics theory can be applied. A simple validation of this is that a single motor reaching the tip increases the length by 1.25 nm in our simulation with default parameters, and it takes 4.5 ns for a diffusing motor's mean square displacement to equal 1.25 nm, which is negligible compared to the roughly 18 s it takes to diffuse back to the base.)

The strategy for deriving an expression for steady-state length is to determine the expected flux of diffusing motors arriving at the base, equate the flux to the number of motors diffusing from the tip (following our assumptions that injection time and active transport time are very small compared to diffusion time), convert that flux into a dynamic growth term, and then find the steady state at which this growth is balanced with the decay term.

The resulting expression for steady-state length is

$$L_{ss} = \left( \frac{2ND\delta L}{d} \right)^{\frac{1}{2}}, \quad (1)$$

where  $N$  is the number of diffusing motors,  $D$  is the diffusion coefficient,  $\delta L$  is the increment of flagellar growth when a motor reaches the tip, and  $d$  is the decay rate. The derivation is below.

The time it takes a random walker to move a root mean square distance  $L$  is

$$t = \frac{L^2}{2D}.$$

The current of motors  $I$  reaching the base is equal to the number of diffusing motors  $N$  divided by the average time it takes to diffuse to the base,

$$I = \frac{N}{t} = \frac{2ND}{L^2}.$$

In the approximation in which motors that have reached the base immediately transport back to the tip, the flagellum grows at a rate given by the current of motors reaching the base multiplied by the growth increment per motor  $\delta L$ . The competing decay term  $d$  is length-independent:

$$\frac{dL}{dt} = \frac{2ND\delta L}{L^2} - d.$$

At steady state,  $dL/dt = 0$ , so we can solve for the steady-state length  $L_{ss}$ :

$$L_{ss} = \left( \frac{2ND\delta L}{d} \right)^{\frac{1}{2}}.$$

An identical result can be obtained by solving the diffusion equation for appropriate boundary conditions and expressing the motor return rate in terms of the flux at steady state.

This model predicts that the steady-state length of the flagellum is proportional to the square root of its diffusion coefficient, motor number, and unit length increase per motor. It also predicts that steady-state length is inversely proportional to the square root of the decay rate. Note that because the model proposed does not invoke any unknown transducer molecules or pathways, but instead directly represents all of the molecular players, there is no need for any undetermined constant of proportionality.

benefit of simple model

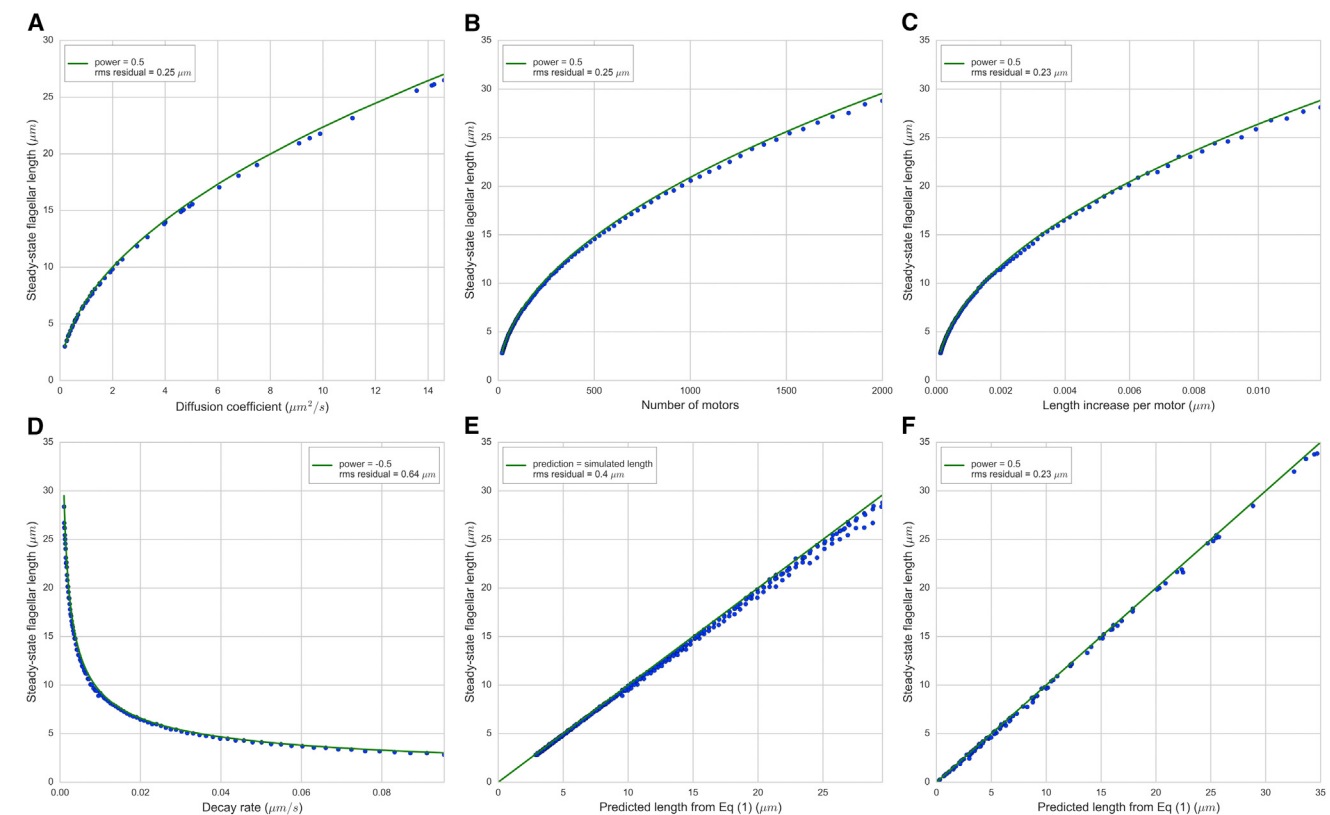


**FIGURE 3** Comparison of analytical solution of diffusion equation to agent-based model. Each plot shows the steady-state lengths given by Eq. 1 and agent-based simulations by varying a single parameter at a time. The varied parameters are: (A) diffusion coefficient  $D$ , (B) number of motors  $N$ , (C) length increase per motor  $\delta L$ , (D) decay rate  $d$ , and (E) plot of length predicted from Eq. 1 compared to simulation results. In this panel, all individual parameter variations simulated in the plots from (A)–(C) and (E) are plotted in the same graph, with the parameter set used in each simulation inserted into Eq. 1 to yield the predicted length, then plotted against the final steady-state length simulated by the agent-based model. (F) Simulated steady-state lengths of flagella are given with randomly selected values for  $D$ ,  $N$ ,  $\delta L$ , and  $d$ . In this panel, all four variables were simultaneously varied, instead of varied individually as in (E). Each subplot has the curve predicted from Eq. 1 superimposed onto the data in green, along with a root mean square value for the residual between the simulated lengths and the prediction. The points in all panels were uniformly sampled in log space, so there is the same number of points between the default and one order of magnitude below as there are between the default and one order of magnitude above. To see this figure in color, go online.

By running simulations in the agent-based model over a range of parameters, we can verify that this relation matches the results of fine-grained agent-based simulations (Fig. 3). Specifically, we see close matches between theory and simulation as we vary diffusion coefficient (Fig. 3 A), number of motors (Fig. 3 B), length increase per motor (Fig. 3 C), and decay rate (Fig. 3 D). When simulated lengths are plotted versus the prediction of Eq. 1, we observe a virtually identical match (Fig. 3 E), with <5% deviation on average. This is also true when parameters are varied in combination (Fig. 3 F). To simulate our assumptions, these simulations have an avalanching threshold of one motor and an active transport speed of 200  $\mu\text{m}/\text{s}$  (enough to go the entire length of the flagellum in one time step). The similarity between the predictions of Eq. 1 and the simulated lengths indicate that Eq. 1 accurately describes the length of diffusion-regulated flagella. For all parameter combinations simulated, a single steady-state length is achieved. We used a **Markov model** to verify that

more info

the presence of a unique stable steady-state solution is intrinsic to the model (see Fig. S1).

Equation 1 above describes the steady-state flagellar length in the limit of instantaneous injection and active transport. To determine whether deviations from these assumptions might have a significant effect over a large region of parameter space, we simulated flagella with a wide range of the parameters not included in Eq. 1. Specifically, we scanned over IFT velocity and avalanching parameters and held all other parameters constant. The effects on steady-state length are displayed in Fig. 4. The Weibull distribution used to determine avalanching dynamics has two parameters: the power and the prefactor. Fig. 4 A shows the final lengths generated by varying the power, and Fig. 4 B shows the final lengths generated by varying the prefactor. Both indicate that the Weibull parameters do not significantly affect length, implying that the specifics of IFT injection do not affect final length. This can be understood by considering that the avalanching dynamics dictate that on average, larger injections lead to more time between injections. So, in steady state, the

only the avalanching threshold (and the velocity of motors) is important for the final length of the flagellum

Diffusion as a Ruler

average build rate of the flagella is independent of avalanching parameters. The avalanching threshold (Fig. 4 C) affects the final length because increasing the threshold increases the average number of motors in the base at any given time, thereby decreasing the number of diffusing motors and decreasing the steady-state length. Essentially,

$$N_{\text{flagellum}} = N - N_{\text{thresh}}. \quad (2)$$

The velocity of motors only affects the final length in low velocity regimes (Fig. 4 D). This is also due to the effective decrease in motors in diffusion. The number of motors in active transport, diffusion, and the base combined is conserved, so the longer a motor is in active transport or waiting at the base, the less often it is diffusing. To calculate the fraction of motors inside the flagellum in diffusion, we must consider the time it takes to complete active transport and diffusion, and treat this as the probability of drawing a diffusing motor. The time it takes for a particle to diffuse a root mean square distance  $L$  is  $L^2/(2D)$ , and the time it takes

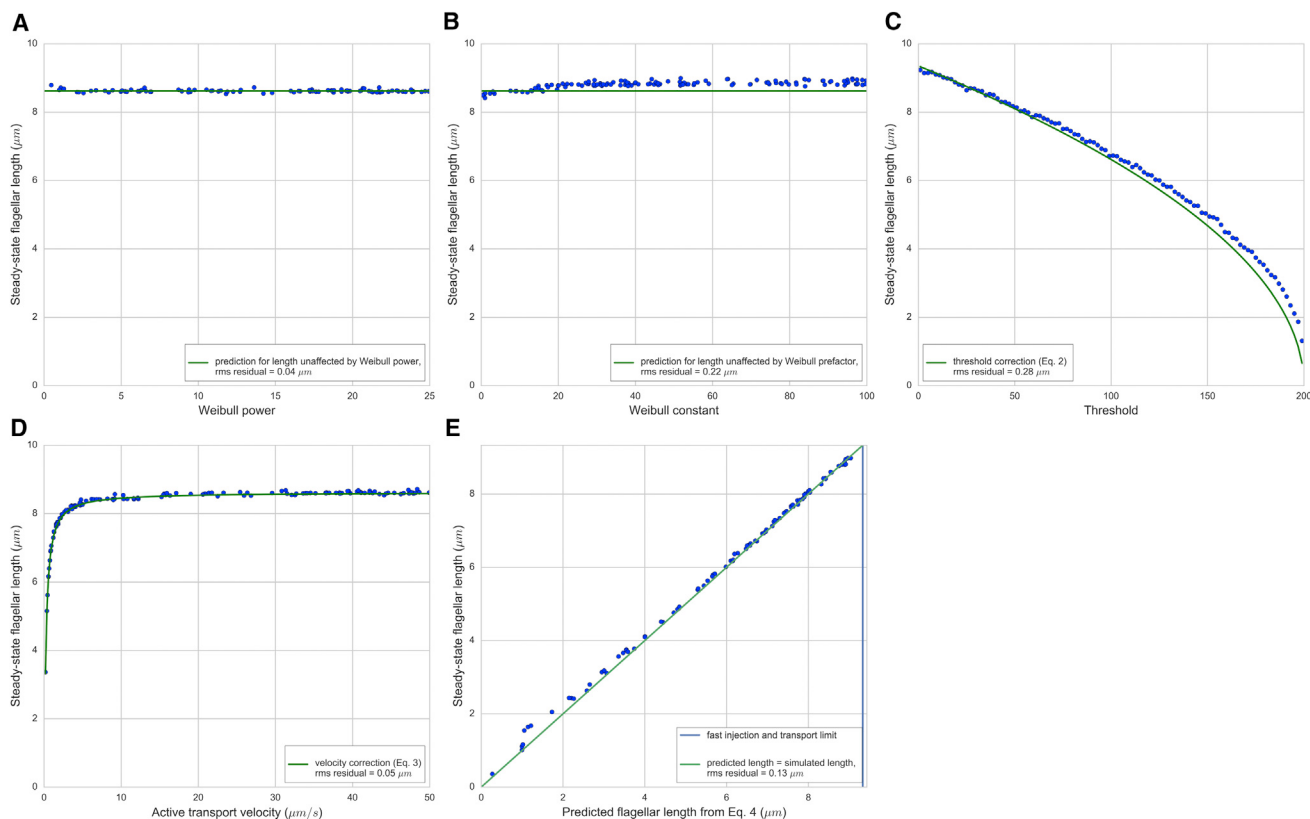


FIGURE 4 Effect of remaining parameters on steady-state length. Each plot shows the steady-state lengths for simulations altering variables not included in Eq. 1. The varied parameters are: (A) Weibull distribution power, (B) Weibull distribution prefactor, (C) avalanching threshold (number of motors built up in the base required to trigger an avalanche), and (D) velocity of motors in active transport of IFT. The varied parameters in (A)–(C) are involved in the avalanching mechanism. Each panel has a line in green superimposed on the data representing the effect that the given variable has on steady-state length. In (A) and (B), we claim there is no significant effect. In (C), Eq. 2 is superimposed on the simulated data, and (D) has Eq. 3 superimposed. In (E), the threshold and transport velocity are both randomly generated and simulated, and Eq. 4 is superimposed. Root mean square residuals between the simulated lengths and the predictions are displayed in the legends of each panel. To see this figure in color, go online.

for a motor with constant speed  $v$  to move a distance  $L$  is  $L/v$ . The sum of these two is the mean total time to complete active transport and diffusion, so the probability of drawing a diffusing motor is

$$p_{\text{diffusing}} = \frac{\frac{L^2}{2D}}{\frac{L}{v} + \frac{L^2}{2D}},$$

assumption: two flagella equalize each other

which simplifies to

$$p_{\text{diffusing}} = \frac{1}{1 + \frac{2D}{Lv}}. \quad (3)$$

To confirm the relations in Eqs. 2 and 3, we superimposed the curves onto Fig. 4, C and D, respectively. The low root mean square residuals to these curves shows that these corrective terms adequately describe the changes in length associated with avalanching threshold and transport velocity. Combining Eqs. 2 and 3 yields an overall correction for the  $N$  used previously for the number of motors used to predict steady-state length:

$$N_{\text{eff}} = (N - N_{\text{thresh}}) \left( \frac{1}{1 + \frac{2D}{Lv}} \right), \quad (4)$$

where  $N_{\text{eff}}$  is the effective number of motors, i.e., the number of motors in diffusion.

Fig. 4 E shows the steady-state length in simulations with random values for velocity and avalanching threshold. The predicted length values are generated using Eq. 1 with the

value for  $N_{\text{eff}}$  plugged in for  $N$ . Note that the final length is included in the expression for  $N_{\text{eff}}$ , so instead of solving for  $L$  directly in the prediction, we used the final length from the simulation in the expression for the prediction, because our goal is just to show the validity of the equation.

## Coordination of multiple flagella

The model as it stands only includes a single flagellum, whereas *Chlamydomonas* cells have two. Experimental evidence shows that the two flagella in a given cell interact. Indeed, one of the most dramatic experiments in the length control literature is the demonstration that cells can equalize the lengths of their two flagella after one has been cut (called the “long-zero” experiment) (2). This is crucial for swimming, but more importantly, it creates the striking visual impression that each flagellum knows how long the other one is. In models that involve length sensor pathways, this coordination can be explained by some sort of molecular cross talk between the length sensing pathways. In the diffusion-based length control model described here, there is no length-sensing pathway per se, and instead length influences growth rates simply by the timescale of diffusive return. This raises the question of whether the model can account for length equalization.

To answer this question, we expanded the model to simulate two flagella competing for a common pool of material (Fig. 5). We imagine the material in question to be tubulin, but in fact the axoneme is a complex structure with many proteins in it, some of which are involved in its assembly, and we do not currently know which axonemal structural protein is the limiting factor in terms of flagellar length. To include the effect of pool depletion in our model, we

problem: no cross talk in the diffusive model  
idea: two flagae one pool

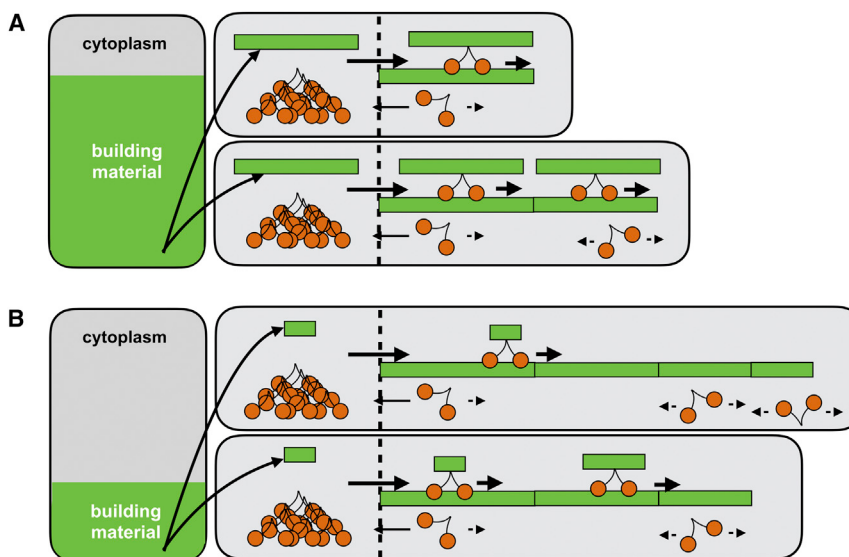


**FIGURE 5** Two-flagella model. Diagram of model is expanded to include a second flagellum and a shared pool of material. The amount of building material each motor carries is proportional to the remaining amount of shared material in the pool (Eq. 5). (A) Early on in the growth of the flagella, the amount of material is high, and therefore the amount of building material each motor carries is high. (B) Later in the growth of the flagella, the material pool has been partially depleted to build the flagella, so the build size per motor has decreased. To see this figure in color, go online.

modification in the simulation:  
the length of growth is proportional to  
the free pool size

changed the amount that the flagellum grows when a motor reaches the tip from a constant to a proportion of the size of the free pool. For a total pool size  $T$ , flagellar lengths  $L_1$  and  $L_2$ , and a constant of proportionality  $k_{\text{pool}}$ , the build size of an injected motor becomes

$$\delta L = k_{\text{pool}}(T - L_1 - L_2). \quad (5)$$

Note that we express the size of the pool  $T$  in units of length, so the pool can be thought of as the maximum possible total flagellar length. In the early growth phase,  $L_1$  and  $L_2$  are small, so the build size of an injected motor is big (Fig. 5 A). Later, the flagella are longer, so the smaller amount of available material leads to a smaller build size (Fig. 5 B). Note that the building material does not have to be fully depleted for the flagella to stop growing, because the kinesin availability is still in competition with the constant decay.

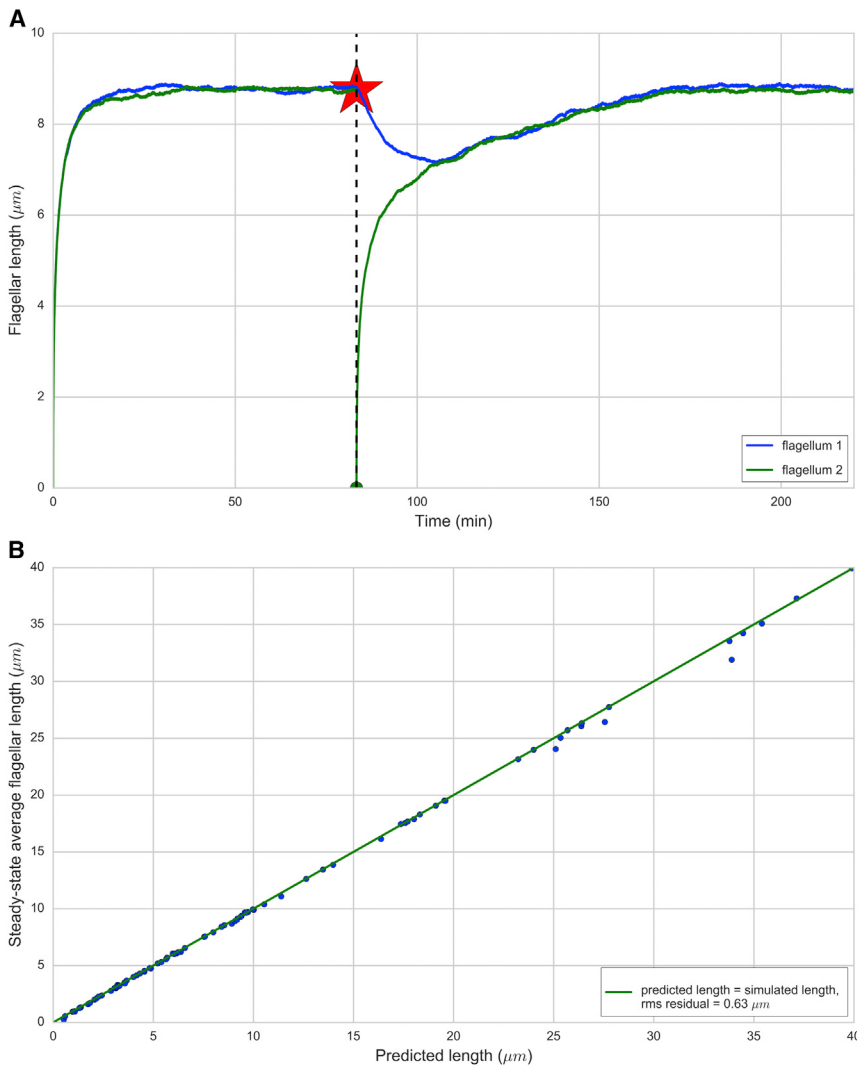


Fig. 6 shows the results of the new simulation. To simulate the long-zero experiment, we simulated a two-flagella cell until it reached steady state then set the length of one flagellum to zero (Fig. 6 A). The length of the cut flagellum was subtracted from the total pool size, because the flagellar material gets lost after being cut. At this stage, we increased the pool size slowly over time until it returned to its original value. The cut flagellum then grows as the long flagellum shrinks. Once they reach the same length, they grow together to steady state. This is consistent with experimental long-zero dynamics. We have a new prediction for final length by replacing the constant  $\delta L$  in Eq. 1 with the pool size-dependent expression in Eq. 5:

$$L_{\text{ss}} = \left( \frac{2N_{\text{eff}}Dk_{\text{pool}}(T - 2L_{\text{ss}})}{d} \right)^{\frac{1}{2}}. \quad (6)$$

Note that in steady state,  $L_1 = L_2 = L_{\text{ss}}$ .

consistent with  
what we expect

FIGURE 6 Simulation with expanded two-flagellum model. (A) Given here is the length-over-time plots for simulation of two flagella competing for a common pool of material. At the time point indicated by the red star, we manually set the length of flagellum traced in green to zero and subtracted its prior length from the pool size. We then resumed the simulation, slowly increasing the pool size until it reached its original value. This is a simulation of the long-zero experiment. (B) Here, we compare the prediction of Eq. 6 to the simulated length. Because the right-hand side of Eq. 6 includes  $L$ , we plotted the left-hand side of Eq. 6 on the y axis and the right-hand side on the x axis. The values for steady-state length were calculated by averaging the steady-state lengths of the two flagella. The green line superimposed onto the data is  $y = x$ , showing where the two sides of Eq. 6 are equal. To see this figure in color, go online.

We validated the equation by simulating over a wide range of parameters and comparing the two sides of the equation (Fig. 6 B). Because  $L_{ss}$  is in both sides of Eq. 6, we plotted the two sides of the equation against each other. On average, there is <5% deviation between the two sides of the equation, indicating that Eq. 6 accurately describes the steady-state lengths of two diffusion-regulated flagella competing for a common pool of material.

The effect of  $T$  on the steady-state length depends on the relative size of  $T$  compared to the other parameters. In regimes with low  $T$  compared to the ratio of build terms and decay terms, the common pool is limiting, and the final flagellar lengths will approach  $T/2$ . In the opposite regime, with high  $T$ , kinesin remains the limiting factor, and the only effect of  $T$  is the steady-state build size.

## DISCUSSION

### Diffusion as a ruler

In this model of length sensing, the cell does not employ a sensor, such as the molecular rulers used for bacteriophage tail length, but rather harnesses the fact that the timescale of diffusion is a function of the distance over which a particle must diffuse. This model is similar to a chemical reaction in which a chemical  $X$  has an assembly term and a degradation term. The concentration of  $X$  over time is given by a simple differential equation, and the steady-state concentration is determined by a combination of biochemical parameters. The flagellum is a similar system because the length has assembly and disassembly terms, and here we predict which specific biochemical parameters are involved (Eq. 1). There is a competition between a growth flux term ( $\delta L^*N^*D$ ) and a decay term  $d$ . Two of these parameters,  $\delta L$  and  $N$ , implicitly contain additional meaningful parameters such as active transport velocity, avalanching threshold, and the size of the shared pool of material (Eq. 6). It is important to note that the square root in Eq. 1 comes from the geometry of the system.

We (19) and others (23) have previously noted that diffusive movement of a signal from one end of the flagellum to the other could be used as a length-measuring scheme. However, these prior models always invoked a “black box” in the form of some machinery that responds to the signal to alter flagellar dynamics. For example, our previous models (19) invoked the idea of a flagellar gate or pore whose opening was regulated by the diffusible signal. Because the nature of this black box was not known, for example its input-output relation, it was not possible to confidently make predictions to be compared with experiments. Our model described here avoids the need for any unspecified black boxes, because the kinesin motor that drives IFT is, itself, the diffusing entity. This allows the parameters of our model to be directly related to experimental predictions. For example, Eq. 6 can be used to determine how variation in different experimentally accessible parameters should alter length.

important difference  
with other models



problem:  
how it  
responds to  
signals?



### Relating model to genetics of length control

The simple mechanism modeled here is sufficient to explain length-dependent IFT injection and stable length control without needing to invoke any new molecular players beyond those already known. But this does not mean that the model works independently of molecular entities. All of the model parameters are determined by the biophysical and enzymatic properties of the known molecular component of the IFT system. It is to be expected that mutations in these molecules can alter flagellar length in predictable ways, potentially allowing the model to help interpret the mechanistic basis of previously described flagellar length-altering mutants.

The diffusion coefficient of kinesin is mainly a property of the size of the molecule and the viscosity of the flagellar matrix, and is thus unlikely to be dramatically altered with point mutations. But it is not hard to imagine that mutations might alter the dynamics of the injection system at the base. Previous research shows that the *lf4* mutant makes the flagellum longer and increases the injection rate but without eliminating the length dependence of injection (16). Such a phenotype could correspond to lowering the threshold of motor buildup required for injection avalanching, which is a parameter in the agent-based model. High thresholds lead to lower injection frequency and lower steady-state length, and low thresholds lead to higher injection frequency and higher steady-state length, as shown in the correction for  $N$  in Eq. 4 and its effect on steady-state length (Eq. 6). This implies that it is possible that the *LF4* gene controls the threshold for how big the pile can be before an avalanche occurs.

Another mutant that we can examine is the *FLA10* gene, which codes for the kinesin motors (9). Temperature-sensitive *fla10* mutants with intact flagella start to lose their flagella when the temperature shifts into the region that disables *FLA10* (9). Growth of *fla10* mutants at intermediate temperatures, which partially disable the motors, leads to intermediate steady-state flagellar lengths (11). In our model, this translates to a reduction in  $N$ , the number of motors in the system. We note that the square-root dependence of steady-state length on motor number (Eq. 1) means that length will decrease sublinearly with decreasing motor number. To reduce length by a factor of 10 would require a reduction in motor number by a factor of 100. Thus, one prediction of this model is that the quantity of motors can be partially depleted, for example in the *fla10* mutation at permissive temperature, and have little detectable effect on length.

 find other examples of studies that confirm this model

### Comparison with other studies

A recent study on mouse axons (24) studies the diffusion of kinesin motors as a mechanism for recycling. Their model for simple diffusion has the same linear distribution of diffusing motors, but they find that the diffusing motors have a nonzero binding rate onto the flagellum from diffusion,

mutants  
can be  
explained  
by the  
model



and therefore the number distribution is exponential. The mouse axon system has a fixed length, but their work provides an example in biology of diffusion and recycling of kinesin.

Models based on diffusion as a length measurement system have been proposed by Levy (23) and by Ludington et al. (16,19). In the model by Levy, the proposed source of the diffusing molecule was the base, not the tip, and it was assumed that the diffusing species directly affected assembly, as opposed to our model in which the diffusing molecule affects transport. In the Ludington 2013 model, RanGTP was the diffusing substance, and the link to injection was indirect, requiring a gating of entry by activated Ran (16). In the diffusion model investigated in Ludington 2015, the identity of the diffusing molecule was not specified and again a transducer system was assumed to couple the diffusive molecule to the injection system (19). Finally, we note that although a strength of our model is that length can be sensed and converted into length-dependent IFT injection without the need to invoke any other molecular players, it has been shown that kinases inside the flagellar compartment do show length-dependent activity (25,26). Likewise, flagellar disassembly can become length-dependent when flagella grow outside of a normal length range (27). It is interesting to consider whether these molecular activities may be dependent on IFT injection or diffusive return.

## Future prospects

A fundamental puzzle of flagellar length control has always been how a molecular signal could be generated that depends on length. Our prior results indicated that IFT injection was length-dependent but did not explain the origin of the length dependence, thus raising the possibility that some complex length-measuring molecular pathway may exist. The results presented above establish that diffusive return of kinesin motors is, at least in principle, capable of providing a length measurement system for regulating IFT injection as a function of flagellar length, without requiring any additional regulatory or sensing components. In other words, the IFT system may contain its own measurement method based on the physics of diffusion. It is interesting to consider whether this type of measuring system could be at work in other linear cellular structures such as microvilli or microtubules.

## SUPPORTING MATERIAL

Supporting Materials and Methods and one figure are available at [http://www.biophysj.org/biophysj/supplemental/S0006-3495\(17\)35046-4](http://www.biophysj.org/biophysj/supplemental/S0006-3495(17)35046-4).

## AUTHOR CONTRIBUTIONS

N.L.H. wrote the simulations. N.L.H., M.T., and W.F.M. developed ideas and worked out math. N.L.H. and W.F.M. wrote the manuscript.

## ACKNOWLEDGMENTS

We thank Greyson Lewis for help with the math and derivations and Ahmet Yildiz for sharing results ahead of publication.

This work was supported by National Institutes of Health (NIH) grant GM097017.

## REFERENCES

- Mohapatra, L., T. J. Lagny, ...., J. Kondev. 2016. Length control of filamentous structures in cells by the limiting pool mechanism. *bioRxiv*. <https://doi.org/10.1101/075655>.
- Rosenbaum, J. L., J. E. Moulder, and D. L. Ringo. 1969. Flagellar elongation and shortening in *Chlamydomonas*. The use of cycloheximide and colchicine to study the synthesis and assembly of flagellar proteins. *J. Cell Biol.* 41:600–619.
- Cole, D. G., D. R. Diener, ...., J. L. Rosenbaum. 1998. *Chlamydomonas* kinesin-II-dependent intraflagellar transport (IFT): IFT particles contain proteins required for ciliary assembly in *Caenorhabditis elegans* sensory neurons. *J. Cell Biol.* 141:993–1008.
- Scholey, J. M. 2003. Intraflagellar transport. *Annu. Rev. Cell Dev. Biol.* 19:423–443.
- Taschner, M., and E. Lorentzen. 2016. The intraflagellar transport machinery. *Cold Spring Harb. Perspect. Biol.* 8:a028092.
- Lechtreck, K. F., J. C. van de Weghe, ...., P. Liu. 2017. Protein transport in growing and steady-state cilia. *Traffic*. 18:277–286.
- Stepanek, L., and G. Pigino. 2016. Microtubule doublets are double-track railways for intraflagellar transport trains. *Science*. 352:721–724.
- Vannuccini, E., E. Paccagnini, ...., P. Lupetti. 2016. Two classes of short intraflagellar transport train with different 3D structures are present in *Chlamydomonas* flagella. *J. Cell Sci.* 129:2064–2074.
- Kozminski, K. G., P. L. Beech, and J. L. Rosenbaum. 1995. The *Chlamydomonas* kinesin-like protein FLA10 is involved in motility associated with the flagellar membrane. *J. Cell Biol.* 131:1517–1527.
- Mueller, J., C. A. Perrone, ...., M. E. Porter. 2005. The FLA3 KAP subunit is required for localization of kinesin-2 to the site of flagellar assembly and processive anterograde intraflagellar transport. *Mol. Biol. Cell*. 16:1341–1354.
- Marshall, W. F., and J. L. Rosenbaum. 2001. Intraflagellar transport balances continuous turnover of outer doublet microtubules: implications for flagellar length control. *J. Cell Biol.* 155:405–414.
- Marshall, W. F., H. Qin, ...., J. L. Rosenbaum. 2005. Flagellar length control system: testing a simple model based on intraflagellar transport and turnover. *Mol. Biol. Cell*. 16:270–278.
- Deane, J. A., D. G. Cole, ...., J. L. Rosenbaum. 2001. Localization of intraflagellar transport protein IFT52 identifies basal body transitional fibers as the docking site for IFT particles. *Curr. Biol.* 11:1586–1590.
- Dishinger, J. F., H. L. Kee, ...., K. J. Verhey. 2010. Ciliary entry of the kinesin-2 motor KIF17 is regulated by importin- $\beta$ 2 and RanGTP. *Nat. Cell Biol.* 12:703–710.
- Hu, Q., L. Milenkovic, ...., W. J. Nelson. 2010. A septin diffusion barrier at the base of the primary cilium maintains ciliary membrane protein distribution. *Science*. 329:436–439.
- Ludington, W. B., K. A. Wemmer, ...., W. F. Marshall. 2013. Avalanche-like behavior in ciliary import. *Proc. Natl. Acad. Sci. USA*. 110:3925–3930.
- Engel, B. D., W. B. Ludington, and W. F. Marshall. 2009. Intraflagellar transport particle size scales inversely with flagellar length: revisiting the balance-point length control model. *J. Cell Biol.* 187:81–89.
- Wren, K. N., J. M. Craft, ...., K. F. Lechtreck. 2013. A differential cargo-loading model of ciliary length regulation by IFT. *Curr. Biol.* 23:2463–2471.
- Ludington, W. B., H. Ishikawa, ...., W. F. Marshall. 2015. A systematic comparison of mathematical models for inherent measurement of

- ciliary length: how a cell can measure length and volume. *Biophys. J.* 108:1361–1379.
- 20. Iomini, C., V. Babaev-Khaimov, ..., G. Piperno. 2001. Protein particles in *Chlamydomonas* flagella undergo a transport cycle consisting of four phases. *J. Cell Biol.* 153:13–24.
  - 21. Engel, B. D., H. Ishikawa, ..., W. F. Marshall. 2012. The role of retrograde intraflagellar transport in flagellar assembly, maintenance, and function. *J. Cell Biol.* 199:151–167.
  - 22. Chien, A., S. M. Shih, ..., A. Yildiz. 2017. Dynamics of the IFT machinery at the ciliary tip. *eLife.* 6:e28606.
  - 23. Levy, E. M. 1974. Flagellar elongation as a moving boundary problem. *Bull. Math. Biol.* 36:265–273.
  - 24. Blasius, T. L., N. Reed, ..., K. J. Verhey. 2013. Recycling of kinesin-1 motors by diffusion after transport. *PLoS One.* 8:e76081.
  - 25. Luo, M., M. Cao, ..., J. Pan. 2011. The phosphorylation state of an aurora-like kinase marks the length of growing flagella in *Chlamydomonas*. *Curr. Biol.* 21:586–591.
  - 26. Cao, M., D. Meng, ..., J. Pan. 2013. Activation loop phosphorylation of a protein kinase is a molecular marker of organelle size that dynamically reports flagellar length. *Proc. Natl. Acad. Sci. USA.* 110:12337–12342.
  - 27. Hilton, L. K., K. Gunawardane, ..., L. M. Quarmby. 2013. The kinases LF4 and CNK2 control ciliary length by feedback regulation of assembly and disassembly rates. *Curr. Biol.* 23:2208–2214.